Radiation-Tolerant, High-Power Density Gallium Nitride Point-of-Load Converters

by

Noah Levi Martin

B.S. Electrical Engineering, University of Pittsburgh, 2019

Submitted to the Graduate Faculty of the

Swanson School of Engineering in partial fulfillment

of the requirements for the degree of

Master of Science in Electrical and Computer Engineering

University of Pittsburgh

2021

UNIVERSITY OF PITTSBURGH

SWANSON SCHOOL OF ENGINEERING

This thesis was presented

by

Noah Levi Martin

It was defended on

November 1, 2021

and approved by

Dr. Brandon Grainger, PhD., Assistant Professor, Department of Electrical and Computer
Engineering

Dr. Alan George, PhD., Professor, Department of Electrical and Computer Engineering

Dr. Alexis Kwasinski, PhD., Associate Professor, Department of Electrical and Computer
Engineering

Thesis Advisor: Dr. Brandon Grainger, PhD., Assistant Professor Department of Electrical and
Computer Engineering

Radiation-Tolerant High-Power Density GaN Drop-On Point-of-Load Converters

Noah Levi Martin, M.S.

University of Pittsburgh, 2021

Modern space missions push the limits of on-board power processing making high current output, power dense converters increasingly more crucial for mission success. Increasing power density and efficiency while reducing the converter size, weight, thermal dissipation, and overall cost has become increasingly more difficult with the radiation-hardened converters that are available. Designers are forced to operate at slower switching speeds in comparison to their commercial counterparts. This paper will present the design, development, and testing of three synchronous buck converter drop-on modules which utilize the EPC 2030, 2218, and GaN Systems GS61008T Gallium Nitride (GaN) High Electron Mobility Transistors (HEMT), inductor DC resistance current sensing, thermal dissipation techniques, and an Analog Devices LTC7800 controller to ensure the success of future small-satellite applications.

Keywords: Point-of-Load, Gallium Nitride, High Electron Mobility Transistor, radiation-hardened, Commercial off-the-shelf, synchronous buck converter

Table of Contents

List of Tables

List of Figures

Preface

I would like to thank Dr. Brandon Grainger, my technical advisor, for his guidance over the past year and a half through my Master's thesis. I would also like to thank Thomas Cook for presenting the idea for this research topic and giving me valuable insight throughout the process of design, simulation, and testing.

Thank you to my parents for their continuous and unwavering support during my undergraduate and graduate studies. Because of your hard work and sacrifice, I have been presented with opportunities I never would have had otherwise. You both have been integral to my success and I cannot thank you enough. To my brothers, thank you for being supportive of my aspirations and always being there for me whenever I have needed you.

I would also like to give thanks for the collaboration of my fellow graduate students in the Electric Power Systems Laboratory and the NSF Center for Space High-performance and Resilient Computing (SHREC).

1.0 Introduction

When satellite missions originally began in the 1950s, spacecrafts had individual mission objectives and satellites had weight capacities upwards of 30 kg. Until the 1980s when microsatellites were implemented, spacecraft weight increased proportionally to mission complexity [1]. When the CubeSat emerged in 1999, many years passed before the CubeSat became popular. As space missions have transitioned from the public sector to the private sector, a paradigm shift in space missions occurred. Now, mission objectives are tailored to cost, schedule, and reduced complexity of the mission. Reduced mission scope and the influx of capital from the private sector have steadily increased the number of CubeSat missions since 2010. In the year 2023, there are projected to be 37 times more CubeSat missions than in 2010 alone [1]. In the next 5 years, SpaceWorks estimates 1,800-2,400 nano and microsatellites will need deployment [2]. As the demands for low-earth orbit (LEO) services like broadband constellations, earth observation and analytics, situational awareness, and on-orbit servicing markets continue to grow, the demand for innovation and funding available within the smallsat sector will grow proportionally [3].

This shifted approach in reduced mission objectives, increased funding, and frequency of deployment forces CubeSats to follow strict specifications to ensure mission success and repeatability. Current CubeSat design specifications define the allowable form factors, weight allocation, and testing requirements for a CubeSat. Form factors vary from 1U, 2U, 3U, 4U, 6U, and 12U with each allowing extra weight capacity. As an example, a 1U CubeSat has a small form factor of 10 cm^3, a weight of less than 1 kilogram, and a cost of less than \$50,000 making size, efficiency, weight, and cost essential to CubeSat mission success [1, 4].

Due to the stringent design constraints of these small-scale missions and the growing volume of CubeSats, there has been a call for radiation-tolerant, power dense, high-efficiency point-of-load (PoL) converters. Typically, radiation-hardened (rad-hard) components have large footprints of greater than 300 mm^2, switching speeds of less than 1MHz, and efficiencies of less than 92 percent at max load [5-7]. A GaN HEMT interfaced with a radiation tested commercial off-the-shelf (COTs) controller uses printed circuit board (PCB) space more effectively and is a significantly cheaper solution in comparison to a rad-hard converter. These radiation-tolerant solutions using wide bandgap devices such as GaN have emerged as the preferred choice in low voltage space applications due to their improved efficiency, capability of higher switching frequencies, and a wider bandgap allowing better performance in radiation environments [8].

The contribution of this work is to develop and test nine all-inclusive, or referred to as "drop-on", GaN synchronous buck converters with 3.3, 1.8, and 1.0V output voltages up to a 10A load. The converters have a mechanical footprint of less than 350 mm^2, and efficiency ratings greater than 80 percent. The nine converters have less than a one percent voltage ripple. These newly developed converters will be compared to the widely used, rad-hard, Texas Instruments TPS50601A-SP converter, in terms of electrical performance and mechanical size. The paper is organized as follows. In section 2.0, we will lay the groundwork of why GaN was chosen and the clear benefits GaN has over silicon. Section 3.0, we will discuss the need for power dense power electronics. In section 4.0, an overall converter design and design parameters utilized for the nine converters will be explained. Section 5.0 will discuss the simulation results as well as the test results of the converters. Then, section 6.0 will cover the applications of the converter and trade-offs of high frequency converters. Finally, section 7.0 will consist of closing remarks in regards to the nine point-of-load converters.

2.0 GaN Technology

Increasing power density and efficiency while reducing converter size, thermal dissipation, and overall cost has become increasingly difficult with the currently available radiation-hardened (rad-hard) silicon converter devices. Aerospace engineers typically must utilize rad-hard electronics to meet reliability standards, but these technologies have limited options and tend to operate at slower switching speeds and lower efficiencies, in comparison to their commercial counterparts. However, Gallium Nitride (GaN) High Electron Mobility Transistors (HEMT) show considerable improvements over current rad-hard silicon power MOSFETs when operating at higher frequencies by reducing on-resistance, and parasitic capacitance while maintaining high reliability in a radiation environment [8].

Three GaN HEMTs were chosen for the buck converter topology. These GaN HEMTs include the EPC2030, EPC2218, and the GS61008T. The characteristics of the GaN HEMTs that were tested in this work are shown in Table 1 and 3D packaging is shown in Figure 1. These HEMTs were chosen for a variety of reasons which will be explained in a later section and combined with the Analog Devices LTC7800 synchronous buck controller to ensure proper operation. [9-11]

2.1 Benefits of Gallium Nitride

GaN devices have a larger band-gap of 3.4 eV compared to silicon which has a band-gap of 1.12 eV [8]. This increase in band-gap allows GaN HEMTs to maintain high blocking and

breakdown voltages while also being capable of operating at higher temperatures compared to silicon [12]. Another benefit of GaN is that the input and output capacitances internal to the HEMTs operation allow for faster switching frequencies, slew rates, and improved efficiencies. GaN is capable of switching frequencies greater than 1 MHz with substantially higher efficiencies than silicon rad-hard FETs due to the reduced internal capacitances and the lack of a p-n junction allows zero reverse recovery loss [8]. In addition, to the higher switching frequencies, the ON-resistance of GaN is significantly lower in comparison to rad-hard silicon FETs due to the development of a two-dimensional electron gas (2DEG) inside the HEMT during operation [13]. As a result of the two-dimensional electron gas, the packaging of a GaN HEMT is significantly smaller than a silicon FET yet it achieves similar ratings in terms of ON-resistance and breakdown voltage.

2.2 Radiation Performance of GaN

In addition to the intrinsic benefits of GaN, GaN HEMTs have proven to be very resilient against harsh environments. In space, electronics become more susceptible to extreme temperatures and radiation effects. Gallium Nitride has a higher melting point and equal thermal conductivity to that of silicon [14]. There are four main types of radiation effects that can destroy electronics. They are total ionizing dose (TID), single event effects (SEEs), dose-rate, and displacement damage [8]. Total ionizing dose is the accumulation of charge within the dielectric structure which changes the threshold voltage of the device over the course of the mission. This effect which degrades silicon device performance is eliminated when deploying a GaN HEMT due to the Schottky metal gate nature of the devices. When an energetic ion passes through a

4

semiconductor device, it leaves behind a series of electron-hole pairs within the substrate. After the creation of the electron-hole pair, errors can occur which can potentially damage the device. In silicon semiconductors, the depletion region is much larger which makes SEEs more prevalent. However, GaN has a much smaller depletion region, thus, a less likelihood of SEEs occurring [8]. Since GaN has a smaller depletion region than silicon it is also less vulnerable to dose-rate radiation effects. Displacement damage is the displacement of charge carriers throughout the semiconductor lattice from neutron or proton particles which reduces carrier mobility within the semiconductors. Testing has been done for TID, SEE, and displacement damage within GaN devices and they have proven robust against high radiation fluences [15].

3.0 Power Density

Power dense electronics are becoming increasingly important to the success of CubeSat missions. These missions are becoming increasingly sophisticated with more processors, greater memory capacity, and increasing power requirements while maintaining the same weight and size constraints. Form factor and weight are critical components in every CubeSat mission. The total mass budgeted for a 2U CubeSat mission is 2 kg while only 0.200 kg was allocated to the mass of the power supply to the entire CubeSat [16].

A common radiation-hardened PoL converter is the TPS50601A-SP. Built by Texas Instruments, the synchronous buck converter is capable of outputting up to 6.7V with a maximum load of 6.0A. The Texas Instruments TPS50601SP-A has a maximum switching frequency of 1.0 MHz, which is on par with silicon power FETs and a large footprint of 317.28 mm^2. The size will further increase because the TPS50601A-SP requires additional passive components to ensure proper operation. Additionally, the TPS50601A-SP has a higher expense due to the radiation-hardened nature of the converter [17]. The TPS50601A-SP has a power density of 62 mW/mm^2 operating at 3.3V, a max output current of 6.0A, and a smaller temperature operating range of -55°C to 125°C, making this converter an expensive and limited choice for CubeSat missions. PoL converter topologies need a solution which allows for higher power density designs, improved output capabilities, and effective ways to dissipate heat with a reduced price per chip.

Table 1: GaN HEMT Parameters

Parameter	EPC EPC2030	EPC EPC2218	GaN Systems GS61008T
Drain-Source Voltage	100 V	40 V	100 V
Continuous Drain Current	48 A	60 A	90 A
Threshold Gate-Source Voltage	1.1 V	1.5 V	1.7 V
Maximum Gate-Source Voltage	6.0 V	6.0 V	7.0 V
On Resistance	3.2 mΩ	2.4 mΩ	7.0 mΩ
Gate Charge	13.6 nC	22 nC	8 nC
Package Type	Passivated BGA Die	Passivated BGA Die	GaN$_{PX}$
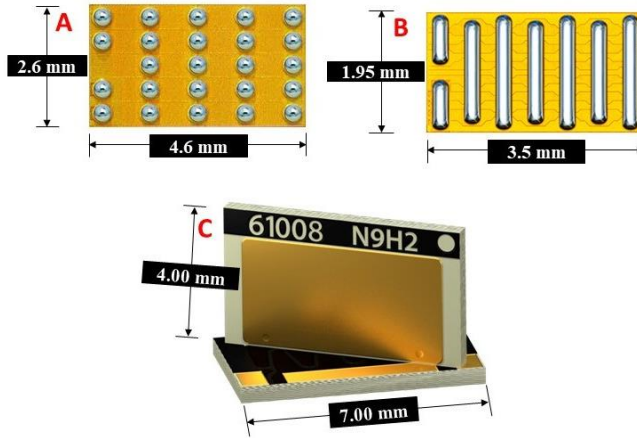
Figure 1: 3D Model dimensions of A) EPC2030, B) EPC2218, and C) GS61008T

The smaller package size and layout of GaN HEMTs decreases parasitic inductances and resistances, thus improving the overall efficiency while increasing the power density of the GaN HEMTs in comparison to the silicon FET [18]. By mechanically attaching the die of the HEMT to the copper pads of the HEMTs the die is then connected directly to the PCB allowing the lowest packaging parasitics. Due to the reduction in size, the GaN HEMTs smaller packaging ensures a lower weight per HEMT proving a valuable alternative to silicon in all CubeSat missions. Additionally, higher switching frequencies achieved by GaN semiconductors allow passive

components to be reduced in size, further improving the power density and reducing the overall weight of the PoL converter [8].

As the power density of the converter is increased the surface area of the converter is reduced, the heat transfer proportionally decreases. In comparison to silicon, GaN devices have more thermal stability at higher temperatures and greater maximum junction temperatures. However, as the junction temperature approaches the maximum junction temperature of 150°C for the GaN devices, the ON-resistance exceeds that of silicon resulting in greater conduction losses [18]. This requires methods of heat dissipation through the use of thermal straps and heat sinks sized to the specific GaN HEMT.

The GaN HEMTs used in this study are the EPC2218, EPC2030, and the GaN Systems GS61008T. The EPC HEMTs are both bottom-side cooled solutions while the GS61008T is top-side cooled. The device characteristics are listed in Table 1 and 3D models of each GaN HEMT are shown in Figure 1 [9-11]. All of the transistors under evaluation are controlled with the Linear Technologies LTC7800 synchronous step-down controller because of its high switching frequency capability of 2 MHz [19]. High switching frequencies will allow a reduction in passive components as previously discussed and thus a reduced mechanical footprint while benefitting from the high slew rates of GaN HEMTs providing improved transient performance of the PoL converter.

4.0 High Frequency Converter Design

This section covers the converter schematic and the PCB layout. The goal of the design was to reduce parasitic losses, improve thermal dissipation, and improve overall efficiency of the converters. A total of nine converters operating with output voltages of 3.3, 1.8, and 1.0 V were developed and tested using three different HEMTs.

4.1 Synchronous Buck Converter Topology

A synchronous buck converter topology was chosen for the design of the converters. This topology uses one commercial off-the-shelf controller to control two HEMTs instead of the traditional buck converter that uses one HEMT and a diode. The two switching GaN HEMTs reduce the losses of the standard buck topology by removing the voltage drop and reverse recovery of a standard diode. By using GaN, additional power savings can be realized because of the reduced parasitic capacitances and lower on-resistance compared to silicon. In doing so, the topology can operate more efficiently. However, a synchronous buck controller allows a shoot-through condition during transitions which can become a problem when driving the GaN HEMTs. This requires a controller with built-in dead-time control to ensure this state is never achieved. The synchronous Buck topology is shown in Figure 2.
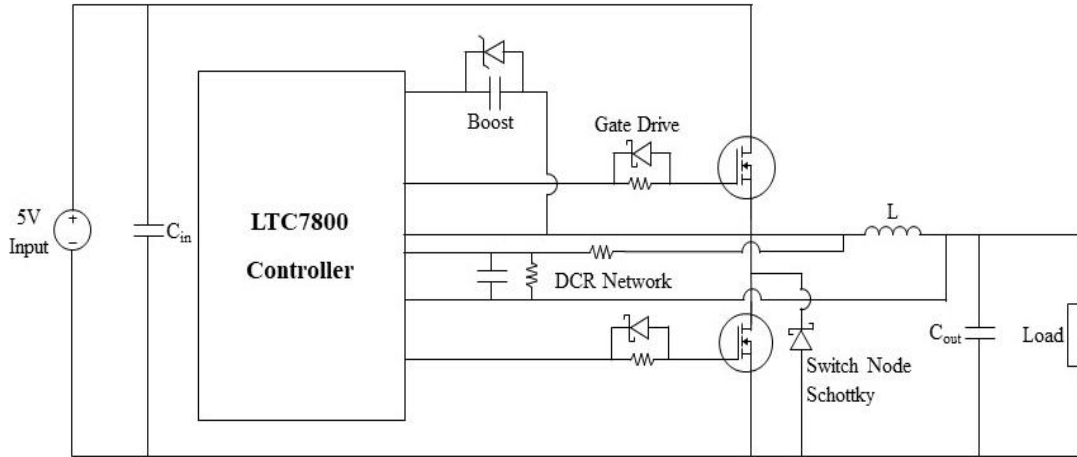
Figure 2: Topology of LTC7800 synchronous buck converter

4.2 Component and Device Selection

Throughout this section design choices and device selection will be outlined for all passive and active components for the nine GaN converters.

4.2.1 Controller Selection

The Analog Devices LTC7800 is a synchronous buck controller. The controller can operate in a wide range of voltages up to 60.0 V and a phase-lockable frequency up to 2.25 MHz. The LTC7800 has a tunable compensation loop that can be optimized for specific load conditions and transient events. Additionally, the LTC7800 has the ability to soft start or track an external voltage, and provides output overvoltage protection. The LTC7800 has been set up to operate in forced conduction mode to ensure correct operation in light load conditions. The LTC7800 is capable of resistor current and inductor DC resistance current sensing (DCR). The DCR sensing is a more

efficient feedback loop than resistor current sensing. DCR sensing utilizes the parasitic losses of the inductor winding, thus eliminating the need for a costly sense resistor while improving efficiency. Additionally, this specific family of controllers has proven performance under neutron-beam testing and in LEO space systems [13]. The overall circuit topology shown in Figure 2 utilizes the LTC7800 controller parameters listed in Table 2, and the controller is paired with one of the GaN HEMTs listed in Table 1 [9-11, 19].

For the design of the three groups of GaN synchronous buck converters, the same topology design shown in Figure 3 was followed. The LTC7800 was set up with a switching frequency of 2 MHz utilizing the slow start and forced conduction feature. Forced conduction mode creates a fixed output voltage ripple and makes the output ripple independent of the load current. Since the switching noise ripple is constant in forced conduction mode it also lends itself to the easiest filtering techniques but suffers from lower efficiencies at light load conditions.

Table 2: LTC7800 Synchronous Buck Controller Parameters

Parameter	LTC7800
Input Voltage Range	4.0 – 60 V
Output Voltage Range	0.8 – 24 V
Switching Frequency	2 MHz
Gate Drive Voltage	5.1 V

4.2.2 Device Gate Driving

Crucial aspects for driving the GaN HEMTs are avoiding shoot-through, ringing, and the Miller effect during device turn-on and turn-off. For this reason, a gate resistor of 5.1Ω was

11

implemented for the turn-on of the GaN HEMT to ensure the gate is critically damped [20, 21]. However, by making the system critically damped, the voltage at the gate takes longer to converge to the 5.1V drive voltage, causing more power dissipation, but no voltage overshoot. The gate resistance calculation was performed using (1), [21].

$$R_G = 2\sqrt{\frac{L_{eq}}{C_{iss}}} * \frac{\frac{1}{\pi}\ln\left(\frac{V_{DR}}{V_{GS,max} - V_{DR} - \Delta}\right)}{\sqrt{1 + \frac{1}{\pi^2}\left[ln\left(\frac{V_{DR}}{V_{GS,max} - V_{DR} - \Delta}\right)\right]^2}} \tag{1}$$

This resistance allows the drive voltage slew rate to be reduced at turn-on and turn-off periods, reduces the ringing period created by the low pass filter, and prolongs the discharge of the gate-to-drain capacitor. Because of the prolonged discharge, a Schottky diode has been added in parallel with the gate resistor to rapidly dissipate stored charge on the gate of the GaN HEMT. This ensures the minimization of the Miller turn-on effect. In order to eliminate the drift of the high side HEMT during transient events, a Zener diode has been placed in parallel with the bootstrap capacitor. Finally, an additional Schottky diode was placed in parallel with the low side HEMT to prevent overvoltage which could damage the HEMTs. The optimization of these parameters was presented in previous work [13]. A simple topology overview of these optimizations in each of the nine synchronous buck converters is shown in Figure 2.

4.2.3 Passive Component Selection

Each passive component was measured for maximum power dissipation in LTSpice simulations and sized accordingly. The ceramic capacitors within the circuit were selected using a 50 percent derating of the maximum input voltage. The input source of the PoL converter uses two

33 µF capacitors to ensure a clean input signal to the converter and accounts for instantaneous current spikes. To ensure the proper amount of output voltage ripple, the higher output voltage applications (3.3 V, 1.8 V) utilize four 22 µF capacitors whereas the lower voltage application (1.0 V) utilizes four 100 µF capacitors. A Coilcraft 0.11 µH shielded power inductor, XGL4020-111MEC, was used in all of the converter designs. The shielded inductor improves radiated electromagnetic interference (EMI) effects while maintaining a large saturation current of 29 A and an extremely low DCR of 1.7 mΩ. The saturation current is slightly less than the typical 50% derating but necessary to maintain a high-power density, low weight, and high efficiency. To ensure recovery during transient events, the compensation loop was tuned for optimal output response at each voltage output. A schematic of the finalized GaN HEMTs converter is shown in Figure 3.
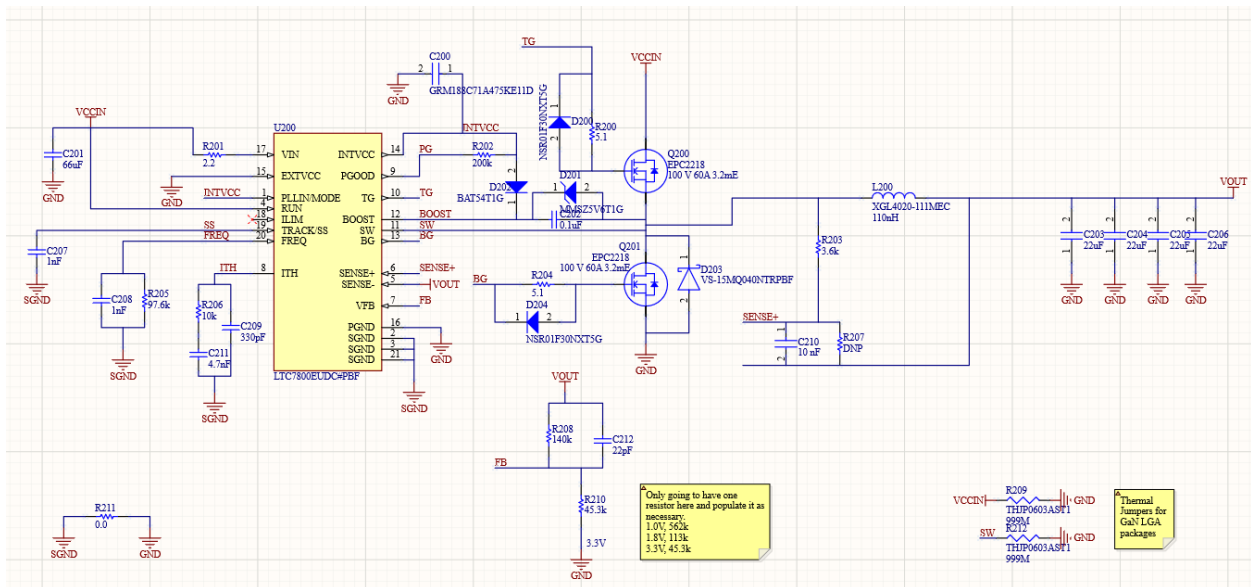

Figure 3: Schematic of LTC7800 with EPC2218 HEMTs for 3.3V operation

4.3 PCB Development & Layout

The circuit boards were developed using Altium Designer. The nine converters were developed and assembled to compare the three different GaN HEMTs against the TPS50601A-SP at various operating points. The mechanical dimensions of the TPS50601A-SP are shown in Figure 4, and the nine newly developed GaN HEMT converters are shown in Figure 5, institute different feedback loop dividers which allow for regulation at the desired output voltages of 3.3, 1.8, and 1.0V.
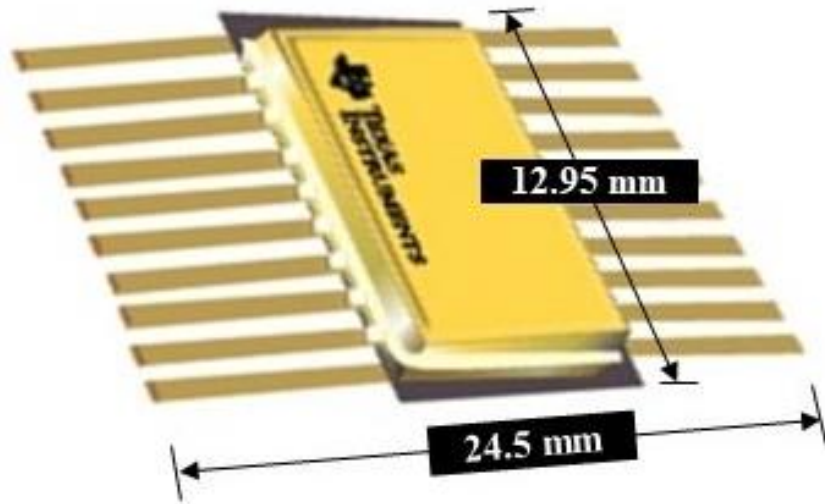

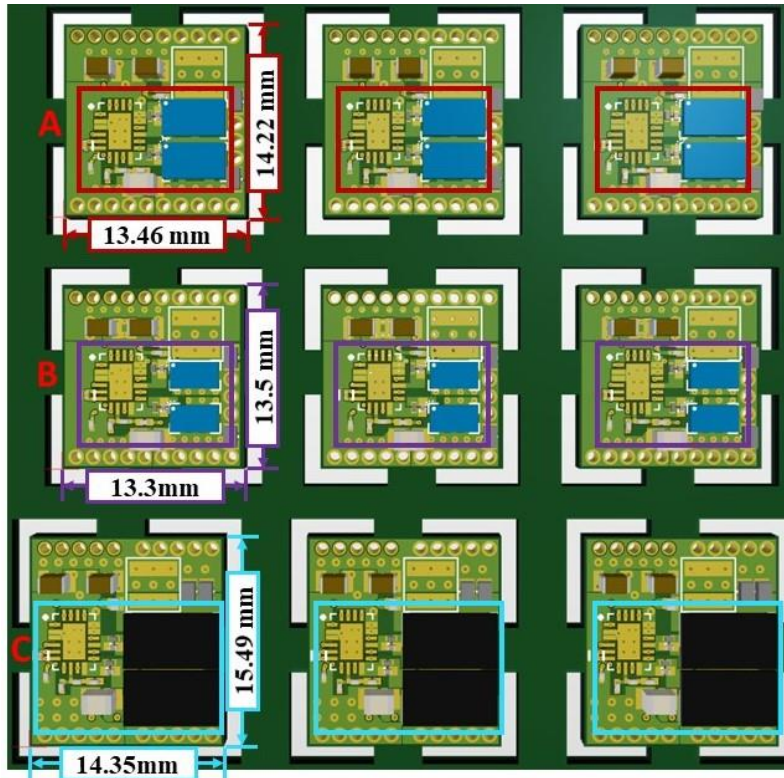**Figure 4: Mechanical dimensions of the TI TPS50601A-SP**

Figure 5: PCB Panel mechanical dimensions of converters under test: A) LTC7800 EPC2030, B) LTC7800 EPC2218, C) LTC7800 GaN Systems GS61008T at 3.3V, 1.8V, and 1.0V output

During the layout process of the three different buck PoL converters, great care was taken when laying out the power path to ensure the minimization of parasitics. Bypass capacitors were placed near the high side HEMT, with a thin PCB dielectric for the smallest power loop inductance. Additionally, the top layer and return path use wide power buses and overlap to ensure the largest reduction in power loop inductance. Reducing the power loop inductance improves the switch node ringing and EMI, drain-to-source voltage stress, and efficiency. Surface mount 0201 gate resistors and Schottky diodes were used at the gate to reduce the gate loop inductance thus reducing gate ringing effects.

However, by reducing the mechanical package size of these drop-on modules and increasing the power density requires thermal considerations to be taken into account. EPC2218, EPC2030 and the GS61008T PCBs utilize new Vishay Dale 0603 package size thermal straps to

dissipate heat into the mating board of the drop-on module connections. The Vishay Dale thermal straps are made of aluminum nitride and have a thermal conductance of 70 mW/°C while maintaining an electrical impedance of greater than 999 MΩ to ensure electrical isolation. Thermal straps were placed on the input voltage and switch node nets. The placement of these thermal straps will dissipate additional heat by providing additional conduction paths through more PCB copper than is typically capable of being thermally connected. Additional vias and headers were added on the EPC2030 and EPC2218 because these HEMTs are bottom-side cooled. This will allow the thermal straps to increase thermal dissipation through headers to the mating board of the drop-on module. In turn, this will reduce the overall temperature of the drop-on PoL converter and allow higher output capacity. The GaN Systems HEMT is a top-side cooled transistor allowing heat sinks to be adhered to the HEMT for increased thermal dissipation. A thermal interface material (TIM) was used to allow the maximum heat transfer to the anodized aluminum heat sinks. The thermally conductive silicone TIM has a thermal conductivity of 5W/m-K.

Size reduction of the drop-on modules was made possible through the minimization of the passive component area. Via-in-pad routing was used in the design to compress the design footprint further. A via-in-pad technique reduces the thermal performance and mechanical connection made to components by creating a hole within the pad. During manufacturing, conductive epoxy filled the vias to enhance thermal performance and ensure rigid board-to-component connection. The traditional via build and via-in-pad with conductive epoxy fill are shown in Figure 6. Combining the size reduction of passive components with via-in-pad routing and thermal dissipation techniques allows for the entire converter to be reduced to the same size or slightly less than the package size of the TPS50601SP-A as shown in the comparison of Figure 4 and Figure 5.
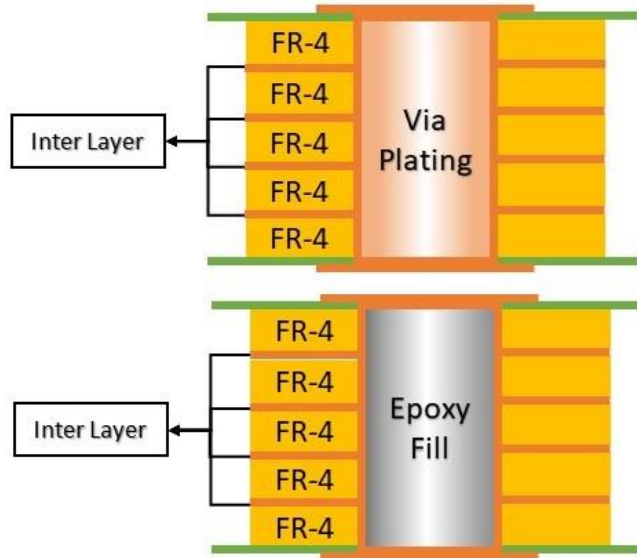
Figure 6: Traditional via w/o epoxy fill and Via-in-Pad w/ epoxy fill

The printed circuit boards follow a 6-layer stackup as outlined in Table 3. The panel of boards was manufactured and assembled by Advanced Circuits. All of the components chosen for the design are 0201 and 0402 packaging with low ESL and ESR values. The input and output capacitances are 0805 packaging to obtain the correct capacitance level necessary for regulation of the input and output.

Table 3: Power dense miniature GaN HEMT PCB Stackup

Layer	Name	Material	Dielectric	Weight (Oz.)	Thickness (mil)
	Top Overlay				
	Top Solder	SM-001			1.0
1	Power/Signal	CF-004		1.0	1.4
	Die Electric 1	2116	Prepreg		8.5
2	GND	CF-004		1.0	1.4
	Die Electric 2	Core	Core		14.0
3	Power	CF-004		1.0	1.4
	Die Electric 3	2116	Prepreg		8.5
4	SGND	CF-004		1.0	1.4
	Die Electric 4	Core	Core		14.0
5	Power	CF-004		1.0	1.4
	Die Electric 5	2116	Prepreg		8.5
6	Bottom Layer	CF-004		1.0	1.4
	Bottom Solder	SM-001			1.0
	Bottom Overlay				

4.4 Test Setup

The nine GaN converters were designed in a 3 x 3 panelization, as shown in Figure 7, for ease of testing the converters. All of the converters were initially tested to ensure the correct parts were populated and proper operation upon startup. After checkout was completed, each converters switching waveforms were simulated and measured on their transient undershoot, overshoot during a 2.5A/µs transient event. Additionally, the output voltage ripple was compared across converters during full load and no-load conditions. All measurements were taken with a Tektronix MSO64 2.5 GHz oscilloscope, Rigol DM3058 digital multimeter, B&K precision 9173B DC power supply, Rigol DL3021 DC programmable load, and a Flir E8 thermal imaging camera as shown in Figure 8. Tektronix TPP1000 passive probes were used with ground spring to reduce ringing on oscilloscope measurements. A TCP0030A current probe was used to measure the input and output current for various testing scenarios.
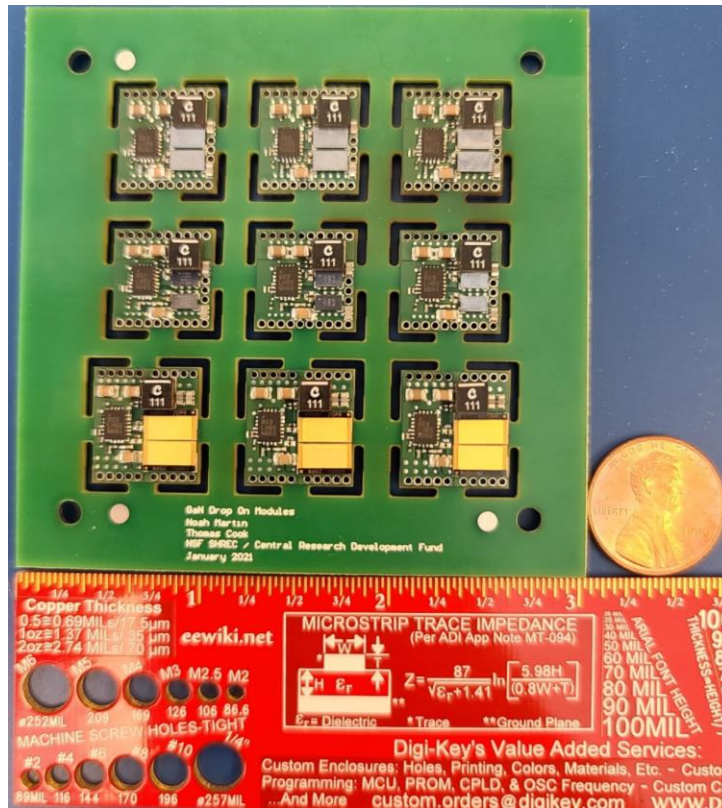
Figure 7: Panelization of nine PoL Converters

Figure 8: Test equipment used for testing various PoL converters

5.0 Converter Results

Within this section, all of the converter simulation results found using LTSpice will be discussed. Then the following section will provide the measured waveforms using the Tektronix MSO064 2.5 GHz oscilloscope. Each section will outline the results of the transient overshoot and undershoot, output voltage ripple, and switching waveforms for each converter.

5.1 Converter Simulations

5.1.1 Converter Waveform Simulation Results

Each GaN converter was simulated using the manufacturer SPICE models from EPC, GaN Systems, and Analog Devices in LTSpice prior to board development. All of the simulations were created to resemble the circuit elements shown in Figure 3 with the exception of R210 which determines the output voltage of the converter. The converters utilized preexisting library models that closely matched to the low-side HEMT Schottky diode, boost capacitor diode, and gate drive diodes. Parasitic values for individual capacitors were implemented in each LTSpice simulation by utilizing K-SIM by KEMET. These similar parasitic models were used to get the closest simulation approximation for efficiency. The simulations did not take into account the parasitics associated with package connections or routing paths necessary for board operation.

The simulations for all three converters show a critically damped gate-to-source drive voltage for each HEMT due to the 5.1 Ω resistor discussed in section 4.2.2. This ensures no

20

overshoot which is a primary concern when driving GaN HEMTs. By reducing the miller-effect with an antiparallel diode, the turn-on of the diode can be viewed in the gate-to-source voltage simulations. However, LTSpice does not take into account the inductances associated with package connections and trace impedances which may cause ringing that cannot be seen within the simulations. The switch node of each converter was simulated to observe the ringing of the switch node. This was done to ensure the absolute maximums of the various HEMTs were not exceeded. The worst-case ringing was observed on the GS61008T at about 7.81V whereas the EPC2030 had the least ringing at 6.8V and the EPC2218 spiked at about 7.21V at the switch node. However, the absolute maximum voltages ratings are slightly higher for the GS61008T, so it is still within the tolerance of the absolute ratings.

In addition to viewing the switching waveforms, the inductor current ripple was viewed in LTSpice to ensure that the controller was regulating within the forced conduction mode. During a loaded condition of 10A, the current ripple of about 2.6A which corresponds to 26% ripple. For the output ripple voltage of the converters, the maximum unloaded voltage ripple was found to be 16.545mV at 3.3V output. This is about 0.5% voltage ripple on the output which is well below the less than one percent voltage ripple targeted. With a 10A load connected to the output and operating at 3.3V output, the maximum voltage ripple was produced by the EPC2218 at about 18.646mV corresponding to 0.56% voltage ripple. The GS61008T and EPC2030 had output ripple voltages less than that of the EPC2218 and can be viewed in Table 5. This shows that the output voltage will regulate fairly well under loaded and unloaded conditions. Similarly, there will be no serious voltage swings during regulation making it a viable option for voltage-sensitive applications requiring loads up to 10A according to simulations.

Each of the converters were simulated under transient conditions. The transient test was performed up to a 10A load with a slew rate of 2.5A/µs. Worst-case overshoot and undershoot were evaluated for each controller. The EPC2030 had the worst overshoot of approximately 184.58mV and the GS61008T had the poorest performance in terms of undershoot at 189.43mV. All of the simulation results for the EPC2030, EPC2218, and the GS61008T operating at 3.3V can be seen in Figure 9, Figure 10, and Figure 11.

(a) EPC2030 high-side (green) and low-side (blue) gate-to-source voltage

(b) EPC2030 loaded inductor current ripple

(c) EPC2030 switch node voltage
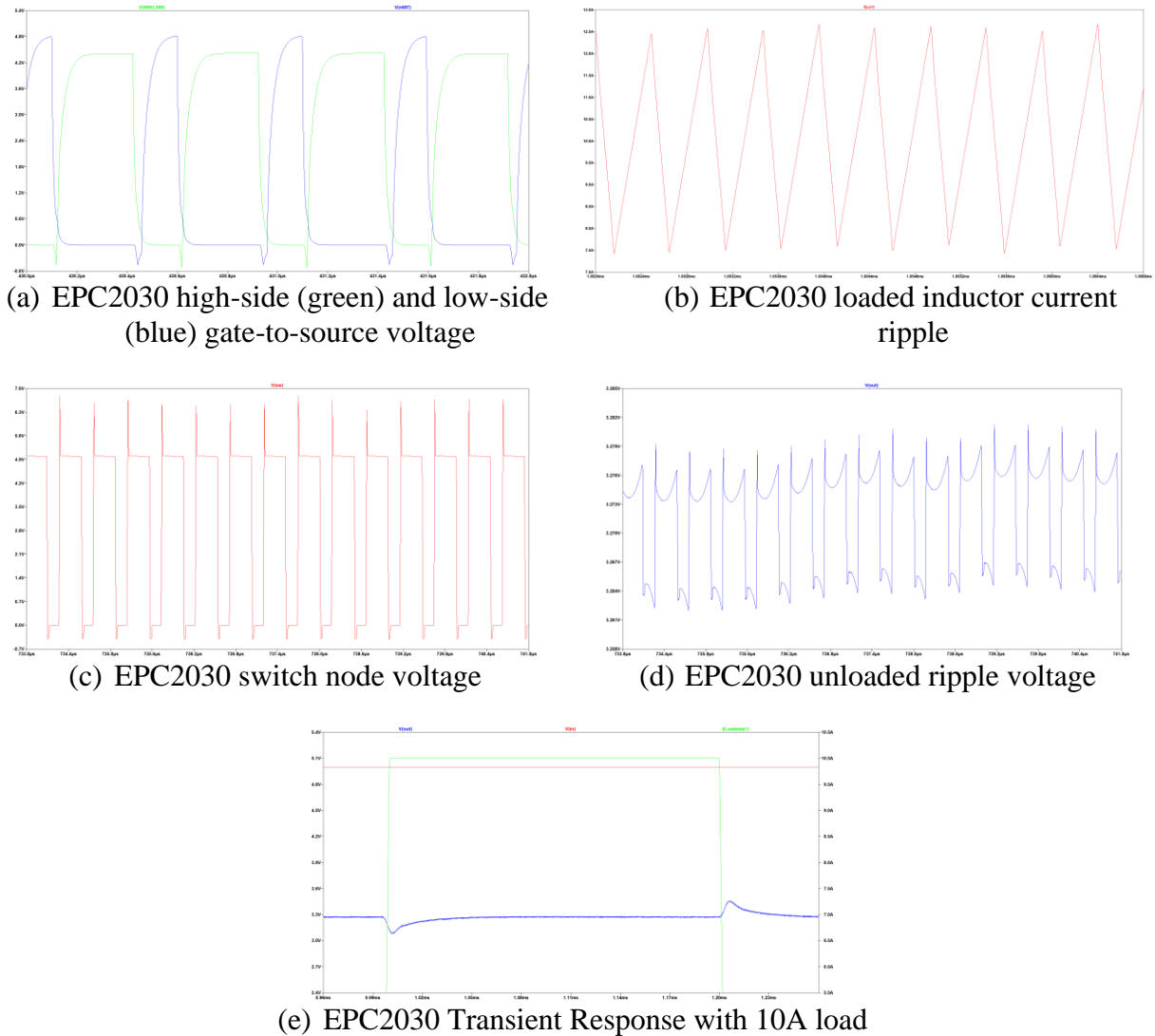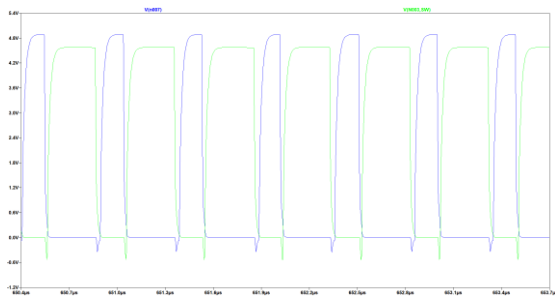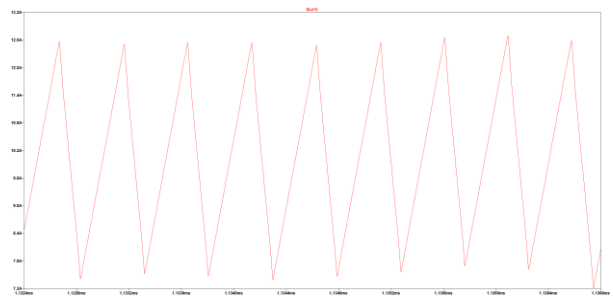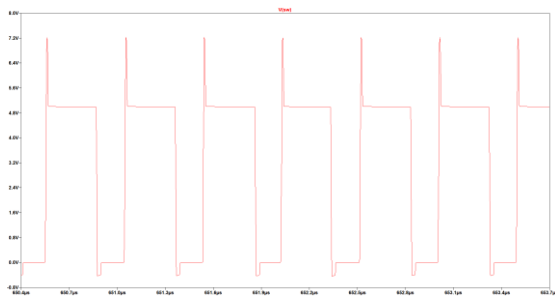
(d) EPC2030 unloaded ripple voltage

(e) EPC2030 Transient Response with 10A load

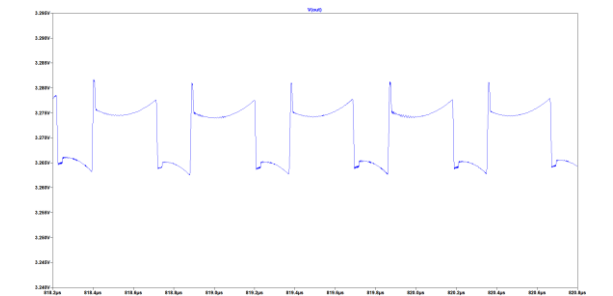**Figure 9: EPC2030 simulated waveforms at 3.3V**

22

(a) EPC2218 high-side (green) and low-side (blue) gate-to-source voltage

(b) EPC2218 inductor current ripple

(c) EPC2218 switch node voltage

(d) EPC2218 unloaded ripple voltage

(e) EPC2218 Transient Response with 10A load

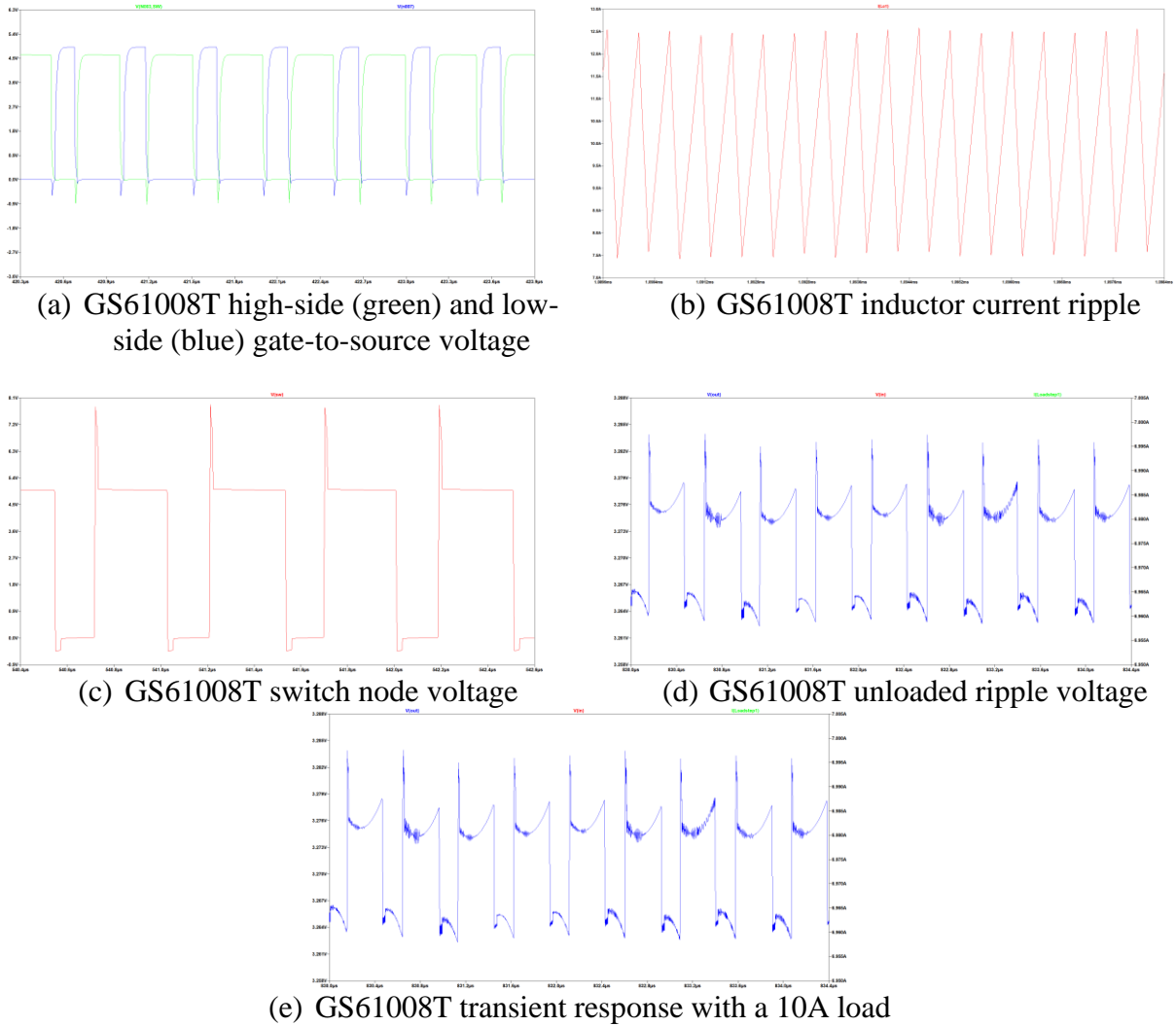**Figure 10: EPC2218 simulated waveforms at 3.3V**

(a) GS61008T high-side (green) and low-side (blue) gate-to-source voltage

(b) GS61008T inductor current ripple

(c) GS61008T switch node voltage

(d) GS61008T unloaded ripple voltage

(e) GS61008T transient response with a 10A load

Figure 11: GS61008T simulated waveforms at 3.3V

5.1.2 Converter Efficiency Simulation Results

The LTSpice schematics that were performed matched the exact topologies shown in Figure 3, which proved to boost efficiency in some cases as much as two percent. Efficiency studies were performed at no-load, light-load, and full-load. In addition, another efficiency study was conducted to observe efficiency versus switching frequency for the power dense GaN converter.

24

Every GaN HEMT simulation was completed using four 22µF capacitors and a switching frequency of 2 MHz for comparison. The peak efficiency in simulation for the EPC2218, EPC2030, and GaN Systems GS61008t was 94.57, 93.36, and 94.85 percent, respectively. Each peak efficiency was centered around a load current of about 4-5 A. For every GaN HEMT with an output voltage of 1.0V, a greater loss in efficiency was observed due to the increasing voltage ripple. The efficiencies shown below in Figure 12, can be increased when using the 100 µF capacitors instead of the 22 µF capacitors. Through the utilization of four 100 µF capacitors at peak efficiency load and maximum load, an increase in efficiency of 0.5 and 0.2 percent was observed for the 1.0V output voltage, respectively.
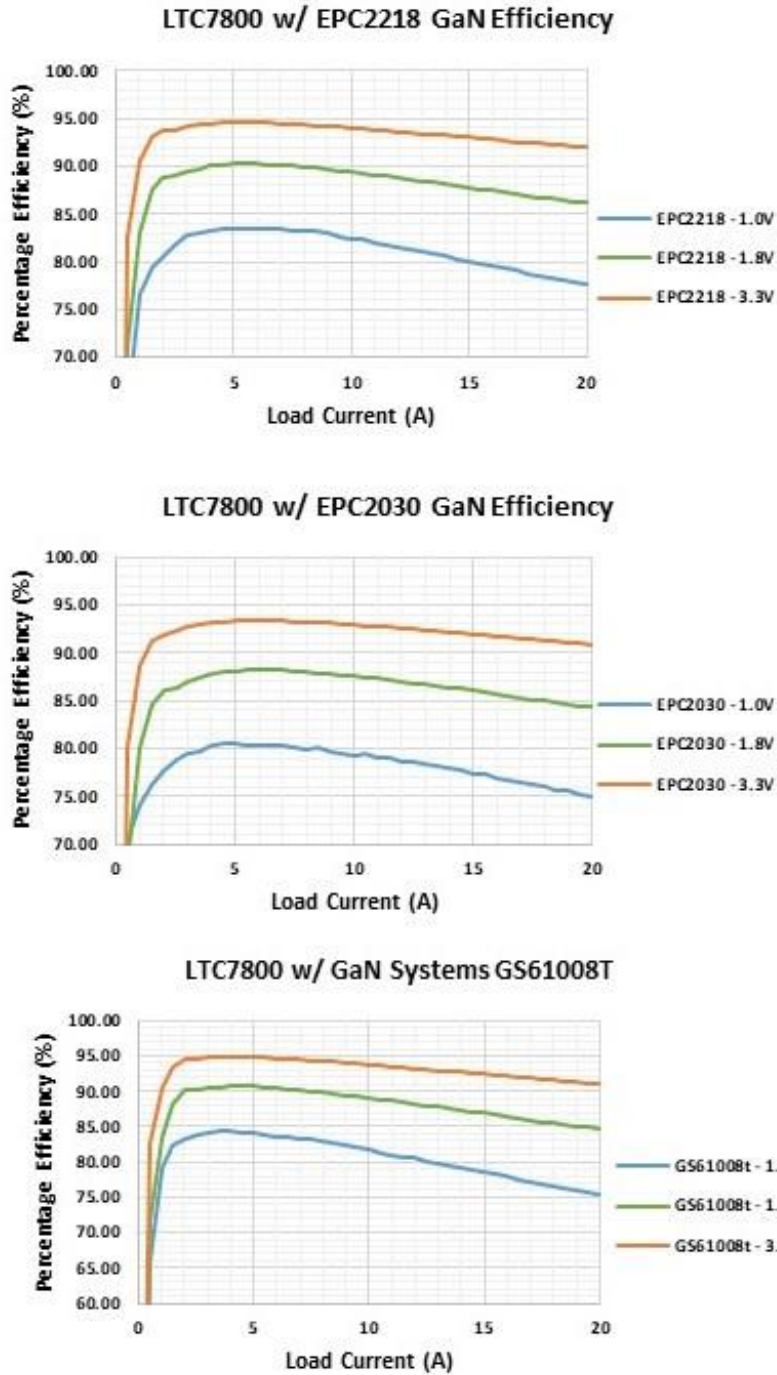
**Figure 12: Simulated efficiencies of GaN Converters at 2MHz fixed switching frequency**

A study was conducted to maintain the same inductor and component sizes while decreasing switching frequency to improve system efficiency of the power dense converter. In

doing so, every element within the circuit remained constant except the compensation loop network and output capacitance. The compensation loop was altered at each frequency step to ensure the control loop and transient performance is maintained throughout the load scenarios. The EPC2030 and EPC2218 largely outperformed the GS61008t during the evaluation. The EPC2218 and EPC2030 efficiencies increased as much as 10 and 12 percent for the 1.0 V output voltage case. Whereas the GS61008t only increased by about 8 percent in the same scenario. However, by decreasing the frequency significantly from the 2 MHz benchmark the saturation current through the inductor increased proportionally. Around 800 kHz an increase in core and saturation losses was observed, but is not greater than the savings in switching losses and, therefore, an increase in efficiency is still obtainable as shown in Figure 13.

Efficiency v. Frequency of GaN HEMTs
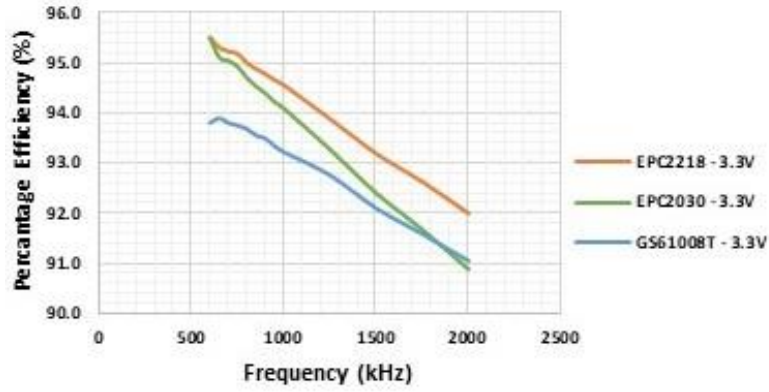
Efficiency v. Frequency of GaN HEMTs
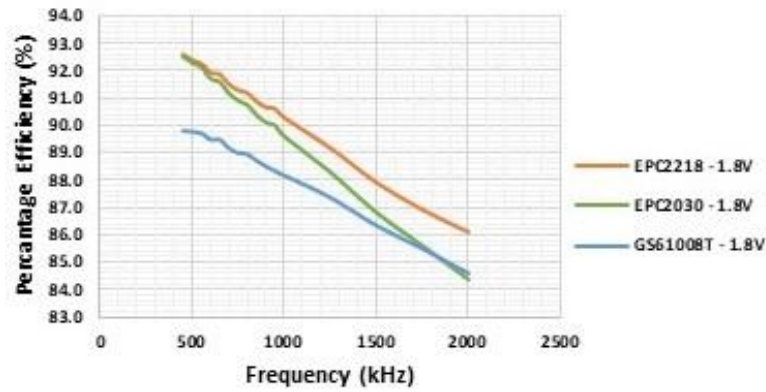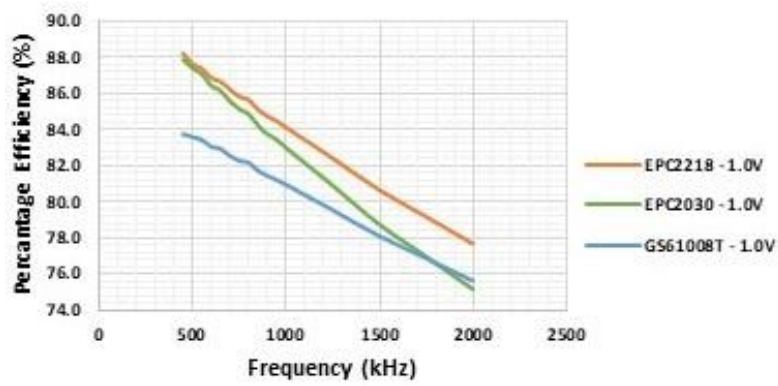

Efficiency v. Frequency of GaN HEMTs

Figure 13: Efficiency v. Frequency of GaN Converters with 20A Load

28

5.2 Converter Hardware Results

5.2.1 Hardware Mechanical Comparison

In comparing the mechanical dimensions of the three different GaN power dense synchronous buck converters to the TPS50601A-SP, we see great improvements. The EPC2218 topology shows the greatest improvement in footprint area of about 43.4 %, while the EPC2030 and GS61008T decreased in size by about 39.6 % and 29.9 %, respectively. However, the GaN PoL converters require more volume than the TPS50601A-SP converter package. This is due to the additional passive and active components used in the GaN converter design compared to only the TPS50601A-SP package. When comparing the weights of each converter, the EPC2218 is the lightest due to the smallest area compared to the other converters. The EPC2218 was about 8.3 times lighter while the EPC2030 and GS61008T were about 7.6 and 7.3 times lighter than the TI TPS50601A-SP. These results can be viewed in Table 4.

Table 4: Mechanical dimensions of the drop-on modules

| Converter Type	Area [mm^2]	Volume [mm^3]	Weight [g]
LTC7800 w/ EPC2218	179.48	1082.62	1.92
LTC7800 w/ EPC2030	191.48	1155.01	2.08
LTC7800 w/ GS61008T	222.35	1341.22	2.18
TI TPS50601A-SP	317.25	766.54	16.0

5.2.2 Converter Hardware Waveforms

The waveforms captured during the simulation of the GaN converters were also captured on the bench. Table 5 outlines the performance of the output ripple during loaded and unloaded conditions as well as the undershoot and overshoot of the GaN converter at their respective output voltages of 3.3, 1.8, and 1.0V.

Both the high side and low side HEMT's gate-to-source voltage was measured to ensure no overshoot during turn-on. As expected from simulation, each waveform shows the antiparallel diode turn-on and turn-off when rapidly discharging the capacitances of the low-side and high-side HEMTs. The switch nodes of each GaN converter were evaluated and performed similarly to the simulations. The EPC2218 had an overshoot of about 7.6V while the EPC2030 and GS61008T had an overshoot of about 7.9V and 8.5V respectively. Each HEMT was within the specified absolute maximum ratings listed in the datasheet. Each switch node showed slight ringing at a transition state, but this is to be expected due to the parasitic inductances and capacitances associated with the PCB.

In comparison to simulations, the GaN converters all performed better than the simulated ripple voltage during no-load conditions except the GS61008T. Each GaN HEMT converter outputs a slightly larger ripple voltage during full-load conditions than simulated in LTSpice. The worst-case performance was shown by the EPC2218 during loaded conditions corresponding to a 1.3% ripple voltage. However, this could be improved upon by increasing the output capacitance as previously discussed in section 4.2.3. The EPC2030 and GS61008T had a ripple voltage lower than the targeted one percent ripple voltage. In terms of transient performance for both overshoot and undershoot, all of the GaN converters had a better voltage response during a transient turn-on and turn-off event than simulated. In contrast to the TPS50601A-SP, the TPS50601A-SP

performed slightly better in terms of both transient and output ripple voltage at the 3.3 and 1.8V operating voltage in comparison to the GaN converters. The GaN converters had better overshoot performance at the 1.0V operating voltage versus the TPS50601A-SP. If better transient performance is necessary for specific applications when using the GaN converters, then the 22µF capacitors can be replaced by the 100µF capacitors as previously discussed in 4.2.3. Additional output capacitance can also be added to the mating board or the GaN converters to accommodate more output capacitance. All of the oscilloscope screenshots can be seen in Figure 14, Figure 15, and Figure 16.
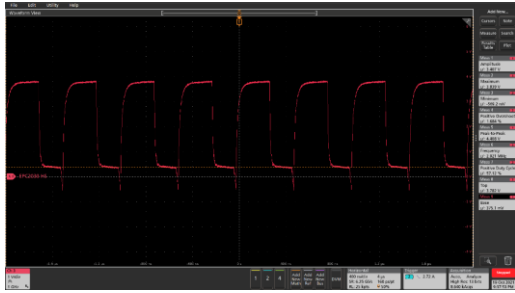
(a) EPC2030 high-side gate-to-source voltage waveform
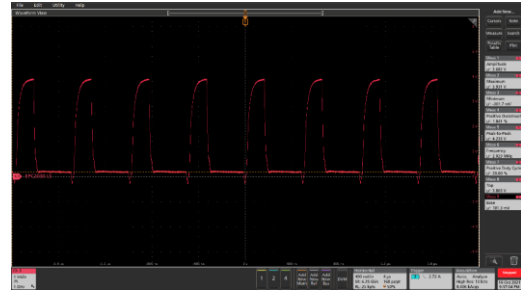
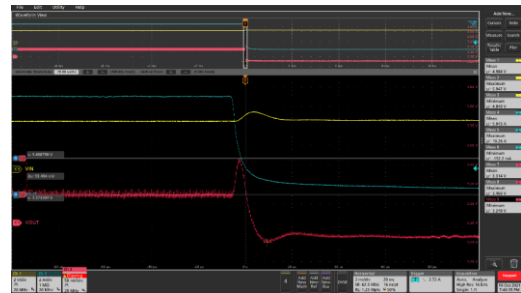(b) EPC2030 low-side gate-to-source voltage waveform
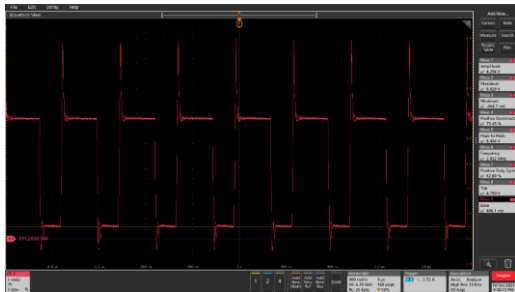
(c) EPC2030 switch node voltage

(d) EPC2030 loaded ripple voltage

(e) EPC2030 undershoot transient event

(f) EPC2030 overshoot transient event

Figure 14: EPC2030 waveforms at 3.3V

(a) EPC2218 high-side gate-to-source
voltage waveform

(b) EPC2218 low-side gate-to-source
voltage waveform

(c) EPC2218 switch node voltage

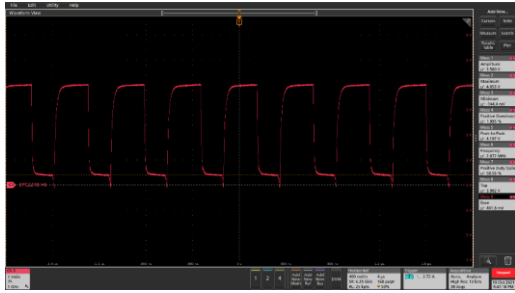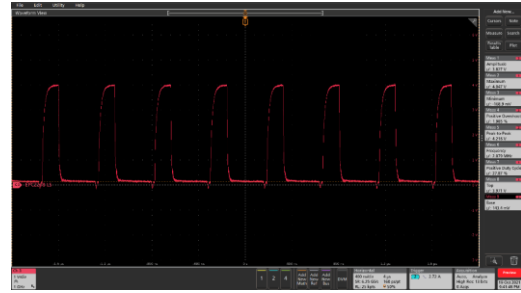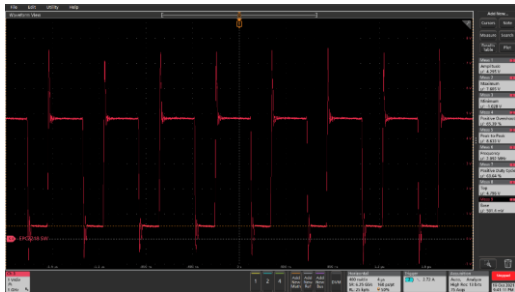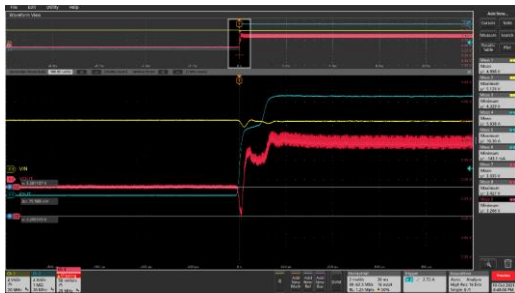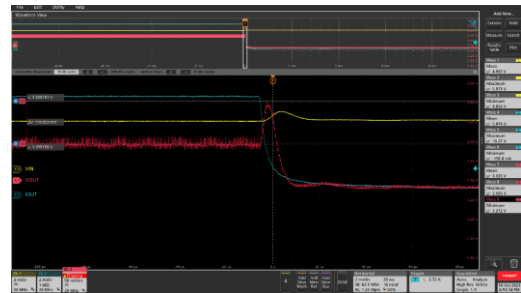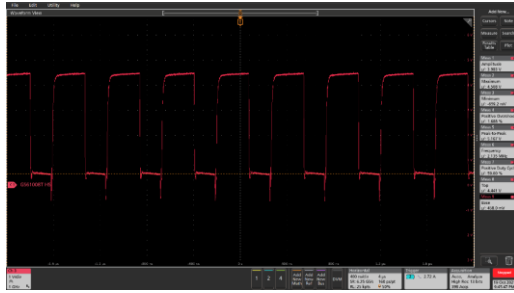(d) EPC2218 unloaded ripple voltage
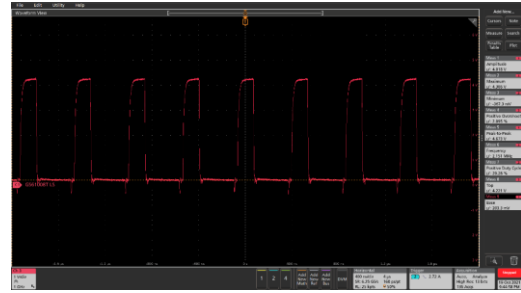

(g) EPC2218 undershoot transient event

(h) EPC2218 overshoot transient event

Figure 15: EPC2218 waveforms at 3.3V

(a) GS61008T high-side gate-to-source voltage waveform

(b) GS61008T low-side gate-to-source voltage waveform
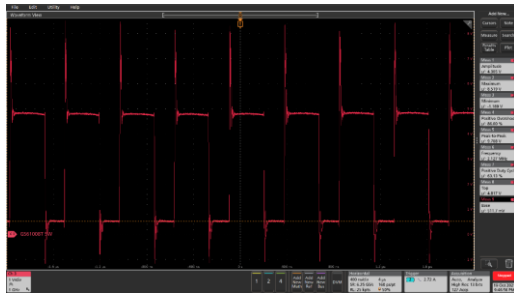
(c) GS61008T switch node voltage
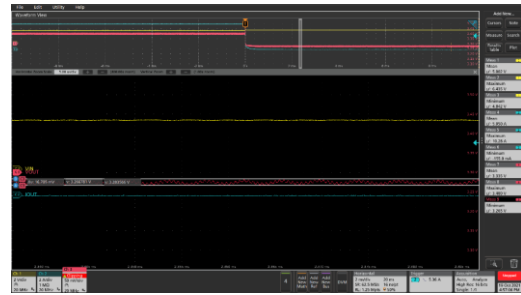
(d) GS61008T unloaded ripple voltage
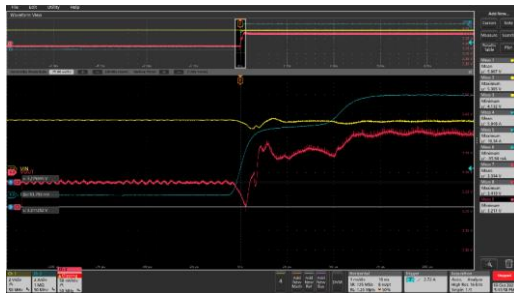
(i) GS61008T undershoot transient event
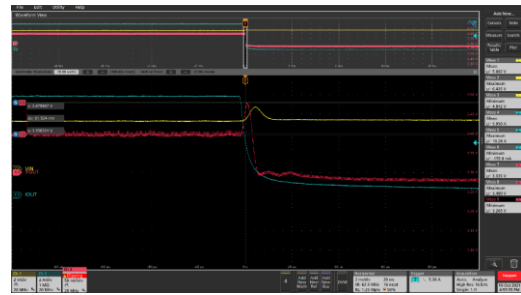
(j) GS61008T overshoot transient event

Figure 16: GaN Systems GS61008T waveforms at 3.3V

Table 5: Output ripple and transient performance of the GaN Converters

Transient Analysis of GaN Converters									
		TPS50601A-SP		LTC7800 w EPC2030		LTC w EPC2218		LTC7800 w/ GS61008T	
		Simulated (mV)	Measured (mV)	Simulated (mV)	Measured (mV)	Simulated (mV)	Measured (mV)	Simulated (mV)	Measured (mV)
Output Ripple	No Load	0.4	1.557	15.462	11.189	16.545	13.74	15.834	16.785
	Load	0.3	3.369	17.774	26.001	18.646	42.53	17.264	19.54
Undershoot	1	10.21	0	83.727	9.049	83.017	13.706	89.447	9.54
	1.8	32.2	0	157.089	23.311	166.607	15.77	164.78	26.34
	3.3	80.3	0	188.53	62.153	184.1	75.59	189.43	63.793
Overshoot	1	83.6	79.104	73.855	20.703	73.953	39.462	86.246	28.718
	1.8	90.7	47.335	135.572	65.322	126.483	73.07	146.063	52.77
	3.3	131.7	84.686	184.58	93.494	182.48	110.023	183.78	81.524

34

5.2.3 Hardware Efficiency Comparison

Each converter was tested at various load conditions similar to the simulation results up to 10A at a 2 MHz switching frequency. The hardware test results match closely to the LTSpice simulation results. As the load current increased, the efficiency of the converters began to drop off because of the junction temperature HEMTs increasing thus proportionally increasing the ON resistance of the HEMT. During testing, the boards were not connected to a mating board, so thermal dissipation was only provided through still ambient air.

With an output voltage of 3.3V, the EPC2218 HEMT outperformed the EPC2030 and GS61008T. The peak efficiency of EPC2218 was found to be 92.93% at a load current of 4.5A while the max load efficiency at 10A was 91.38%. In comparison, the GS61008T and EPC2030 peak efficiency was found to be 92.81% and 92.05% at a load of 3.5A and 4A, respectively, while their max load efficiency at 10A was experimentally found to be 89.26% and 89.84%, respectively.

For an output voltage of 1.8V, the GS61008T had a better peak efficiency performance around 3-4.5A loads of about 88.23%. The EPC2218 and EPC2030 peak efficiencies of 86.58% and 84.29% were centered around 5A and 5.5A, respectively. At max load conditions, the EPC2218 reached an efficiency of 82.72%. The GS61008T efficiency quickly dropped due to the junction temperature increasing and a much larger on-resistance. The GS61008T and the EPC2030 had max load efficiencies of 79.37% and 81.88%, respectively.

In the 1.0V output voltage case, again the GaN Systems GS61008T part has a better peak performance than the EPC parts. The GS61008T had a peak efficiency of 80.98% at a 3A load whereas the EPC 2218 and EPC 2030 had peak efficiencies of 80.40% and 77.16% at 4.5A and 5A, respectively. At maximum load, the EPC2218 performed the best of the three power dense converters followed by the EPC2030 and the GS61008T. These converters operated at efficiencies

of 73.99%, 72.31%, and 68.63%, respectively. All of the efficiency curves of the simulated and experimental power dense converters can be viewed in Figure 17.

In previous work [2], the TPS50601A-SP was evaluated for output voltages of 3.3V, 1.8V, and 1.0V up to the max load output of 6.0A. Using operating voltages of 3.3V, 1.8V, and 1.0V, the TPS50601A-SP operated at peak efficiencies of 93.32%, 86.63%, and 80.30% when supplying a 1.0A load. At max load output, the TPS50601A-SP operated at efficiencies of 79.85%, 76.12%, and 66.12% with a load of 6A. The max load efficiency and peak load efficiency of the GaN converters compared to the Texas Instruments TPS50601A-SP are shown in Table 6.

Power density was also used to compare the hardware of each converter. Each converter was evaluated at the highest output power to compare the converters with similar output characteristics. The TPS50601A-SP package operating at 3.3V has an overall power density of $62mW/mm^2$. The drop-on modules developed through this work performed substantially better than the TPS50601A-SP. The EPC2218 had an overall power density of about $184mW/mm^2$ which corresponds to 196.78% improvement over the TPS50601A-SP. A GaN Systems GS61008T converter had the worst power density improvement at about $148 mW/mm^2$ or a percentage improvement of 138.71%. This can be directly credited to the larger package size of the GS61008T HEMTs. The EPC2030 was second in terms of power density improvement at $175 mW/mm^2$ or 182.26% improvement. Each GaN converter doubled the power density compared to the TPS50601A-SP, and in some cases, like the EPC2218, even tripled the power density while maintaining higher efficiencies than the rad-hard converter. All power density comparisons among the various converters can all be viewed in Table 7.

EPC 2030 Efficency Comparison - 2 MHz
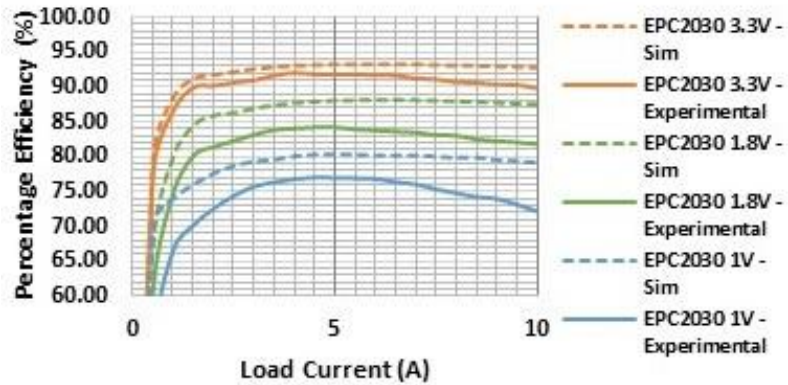
EPC 2218 Efficiency Comparison - 2 MHz
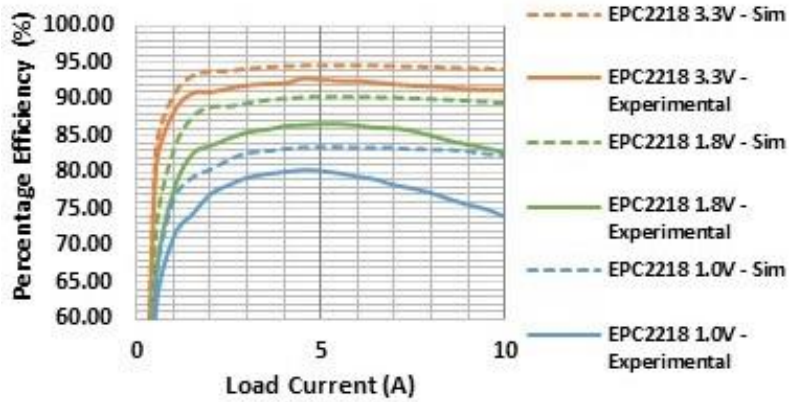
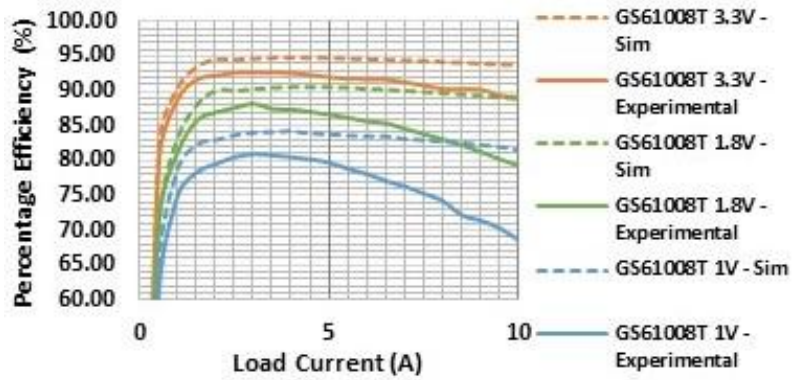## GS61008T Efficiency Comparison - 2 MHz

Figure 17: Efficiency v. Frequency of GaN Converter with 10A Load at 2MHz switching frequency

Table 6: Max and Peak Load comparison of PoL Converters

Efficiency Comparison of PoL Converters				
	Output Voltage	Output Current	Maximum Load Efficiency (%)	Peak Load Efficiency (%)
Texas Instruments TPS50601A-SP	3.3	6.0	79.85	93.32
	1.8	6.0	76.12	86.63
	1.0	6.0	66.12	80.30
EPC - EPC2218	3.3	10.0	91.38	92.93
	1.8	10.0	82.72	86.58
	1.0	10.0	73.99	80.40
EPC - EPC2030	3.3	10.0	89.84	92.05
	1.8	10.0	81.88	84.29
	1.0	10.0	72.31	77.16
GaN Systems - GS61008T	3.3	10.0	89.26	92.81
	1.8	10.0	79.37	88.23
	1.0	10.0	68.63	80.98

Table 7: Power density comparison of PoL converters

Power Density Comparison of PoL Converters						
	Output Voltage (V)	Output Current (A)	Size (mm^2)	Max Load Power (W)	Power Density (W/mm^2)	Percentage Improvement (%)
Texas Instruments TPS50601A-SP	3.3	6.0	317.25	19.8	0.062	-
EPC - EPC2218	3.3	10.0	179.47	33.0	0.184	196.78
EPC - EPC2030	3.3	10.0	188.59	33.0	0.175	182.26
GaN Systems - GS61008T	3.3	10.0	222.35	33.0	0.148	138.71

Thermal performance of these converters is an important aspect to the success of these drop-on modules. As anticipated, the majority of the power loss was near the switching node, which is to be expected due to switching and conduction losses of the HEMTs. During a steady-state no-load condition at 3.3V output, the GS61008T, EPC2030, and EPC2218 converters operate at about 39.5ºC, 46.6ºC, and 44.7ºC as shown in Figure 18. As the current draw from the load increased the efficiency dropped as seen in Figure 17 thus more power was dissipated through heat

generation. As shown in Figure 18, the GS61008T, EPC2030, and EPC2218 converter operated at 121ºC, 124ºC, and 119ºC steady state for a 3.3V output at 10A load which is below the maximum operating temperature of the passive components (125ºC) as well as the max junction temperature of the HEMT (150ºC).
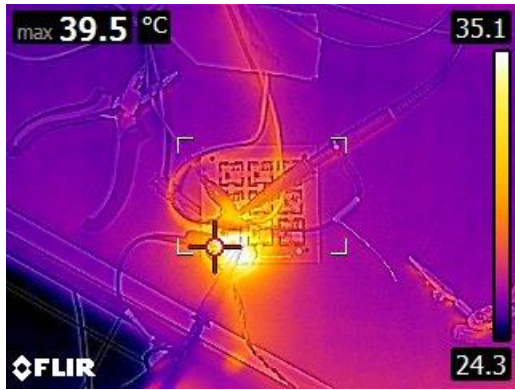
(a) No-load steady-state operation of the GS61008T at 2 MHz for 3.3V output

(b) Loaded steady-state operation of the GS61008T at 2 MHz for 3.3V output
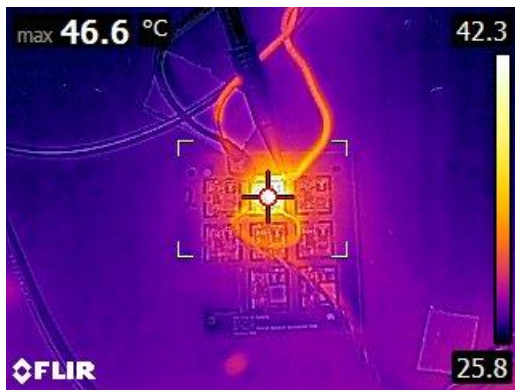
(c) No-load steady-state operation of the EPC2030 at 2 MHz for 3.3V output

(d) Loaded steady-state operation of the EPC2030 at 2 MHz for 3.3V output

(e) No-load steady-state operation of the EPC2218 at 2 MHz for 3.3V output

(f) Loaded steady-state operation of the EPC2218 at 2 MHz for 3.3V output

Figure 18: Thermal steady-state operation of the GaN Converters at 2 MHz

Operating at 1.0V with a load of 10A yielded a max load efficiency of 68.63% for the GaN Systems GS61008T. This indicates a loss of 4.57W at a switching frequency of 2 MHz. By reducing the switching frequency to 450 kHz and maintaining the same inductor for the GaN Systems converter, the max load efficiency was boosted to 74.30% which is about 9.44% less than indicated in the simulation in Figure 13. Additionally, the TPS50601A-SP was found to be 66.16% efficient at max load which indicates almost 8% efficiency improvement using the GaN converters. In turn, the converter is only dissipating 3.46W of power through heat during the steady-state operation of a 10A load. Therefore, this converter is capable of maintaining the same mechanical footprint, regulating with the same output parameters, while benefitting from a reduction in thermal dissipation.

Figure 19: GS61008T with switching frequency of 450kHz
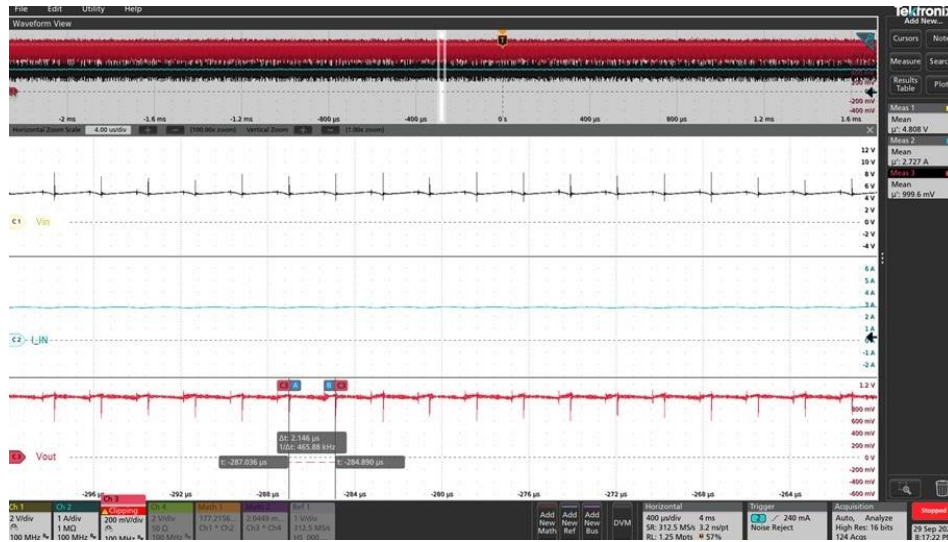
During steady-state no-load operation at 450kHz, the GS61008T converter operates at about 50.0ºC. This increase in temperature compared to Figure 18a can be attributed to the hard switching losses associated with the LTC7800 controller and HEMTs. The hard switching effect can be seen in the output waveform of Figure 19. In addition to the hard switching effect of the

LTC7800 controller, the PCB parasitics amplify the hard switching effects and further reduce our overall efficiency in comparison to the LTSpice simulation of the GS61008T. If a smaller switching frequency is necessary, the XGL4020 Coilcraft family has larger inductor values with the same footprint ensuring the same mechanical footprint, but additional losses will be accrued due to larger DCR. When the GS61008T is under a 10A load, the steady-state operating temperature of the converter is about 113ºC. These results can be seen in Figure 20.
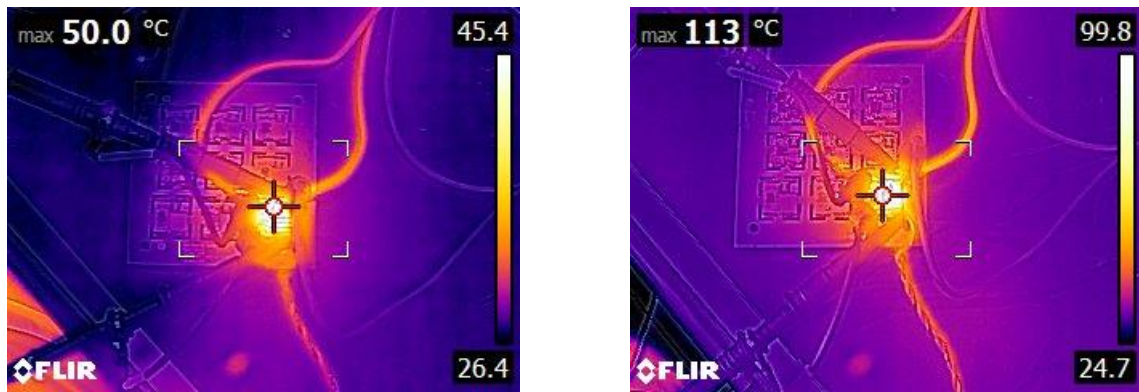
<table>
<tr><td>(g) No-load steady-state operation of the GS61008T at 450kHz for 1.0V output</td><td>(h) Loaded steady-state operation of the GS61008T at 450kHz for 1.0V output</td></tr>
</table>

Figure 20: Thermal steady-state operation of the GS61008T at 450 kHz

Overall, the converters are a vast improvement over the TPS50601A-SP in terms of efficiency and power density. The GaN Converters operate at a switching frequency of 2 MHz which reduces passive components and inductor size. A higher switching frequency also improves the transient performance of the converter. Additionally, using GaN allows fewer losses due to no reverse recovery and reduced intrinsic capacitances. All of these benefits lead to an improved power density, reduced footprint, and higher efficiency. The benefit of the radiation-tolerant, high-power GaN drop-on point of load converters is outlined in Table 5.

6.0 GaN Converter Discussion

Within this section of the paper, a discussion will present possible avenues for the application of the power dense point-of-load converters in addition to possible challenges associated with the converter as well as the cost comparison to the TPS50601A-SP.

6.1 Potential applications

6.1.1 Switching Converter for FPGAs

In the world of reconfigurable computing, FPGA power requirements continue to soar. FPGA fabrics have core voltages lower than 1.0V and tolerances less than 3% while achieving current requirements beyond 30A on the core rail voltage and load transients as fast as 4A/ns [22]. A TPS50601A-SP can only operate up to a switching frequency of 1MHz while outputting a total of 6A maximum with a max load efficiency of 79.85%. Essentially making this rad-hard controller a poor design choice for an FPGA of this caliber. The use of GaN converters with a high current rated HEMT, like the GS61008T or EPC2218, makes these power requirements obtainable at a much higher max load efficiency. The synchronous buck converters presented in this paper show considerable improvements in terms of power density and output capabilities at a high switching frequency while showing strong transient performance. However, additional thermal dissipation techniques will be necessary to achieve the 30A core rails.

6.1.2 Switching Converter vs. LDOs

Low dropout regulators (LDOs) are non-switching converters that can regulate an output voltage for low-power devices while maintaining a clean output signal and simple circuit integration. However, if an LDO is used to power a heavy load, the regulator's resistance will increase proportionally resulting in power dissipation through heat due to the linear nature of the LDO. In addition, the LDO has a limited input voltage range in most applications in comparison to the LTC7800 controller which can handle a variety of input voltages. Primarily LDOs are only useful for low-power applications, but if multiple circuits require various LDOs a synchronous buck converter may be a better solution for the application. The synchronous buck converter has proven to be very effective as a point-of-load converter up to loads of 10A with a high switching frequency. The GaN switching converters footprint has been minimized due to the 2MHz switching frequency while also achieving a low voltage ripple and fast response to transients making these converters well suited for an all-in-one solution to supply multiple auxiliary circuits or a single heavy load.

6.2 High Switching Frequency Trade-offs

The synchronous buck converters operate at a switching frequency of 2MHz whereas most rad-hard converters operate at about 1MHz or less. A higher switching frequency converter dissipates additional power through switching losses requiring better thermal dissipation techniques; however, the higher switching frequency reduces the size of the inductor and capacitors in the converter. The reduction in the inductor and output capacitors reduces the cutoff

frequency of the output filter, thus improving the filtering of high frequency components. Another benefit of the high switching frequency is the improved transient performance and reduced stress on the output capacitors. Lastly, switched currents with high di/dt can produce radiated EMI which could potentially interfere with other circuitry within the mating board. In conclusion, a high switching frequency directly affects the power density and transient performance of the converter at a cost of overall converter efficiency and possible electromagnetic interference.

6.3 Power Density & Efficiency

These drop-on GaN converters cannot be reduced significantly further in terms of size due to the magnetics associated with the topology. The large inductor footprint is the largest or second-largest component on each of the GaN drop-on modules. Through the use of integrated or embedded magnetics, the power density could further be increased. Integrated magnetics is expected to reduce winding losses thus increasing efficiency while maintaining the same inductance. By removing the inductor footprint from the board, additional thermal straps can be used to further dissipate heat throughout other copper layers allowing more surface area for thermal dissipation. Additionally, the efficiency of the proposed converters can be further improved by implementing zero-voltage switching techniques instead of the proposed hard-switching. This will further improve efficiency by decreasing switching losses of the GaN HEMTs and improving the overall thermal performance of the converter. However, this will result in additional passives on the PCB.

6.4 Mechanical and Thermal Challenges

The modular design of the drop-on GaN converters hinges on 20 electrical connections made to the mating board. Based on Samtec's qualification testing procedures like EIA-364-17, 27, 28, and 32, these 20 connections should be sufficient for adhering the drop-on modules to the mating board. Although these connections are intended to dissipate more heat than standard ambient convection, it may be necessary to further study additional heat sinking techniques to enhance the thermal dissipation of the GaN HEMTs and improve output power capabilities. These simulations can be performed using ANSYS Electronics Desktop suite. The header connections will also increase inductance within the power distribution network and introduce potential signal integrity and power integrity issues which may interfere with other circuitry at the desired switching frequency. Shielding may be necessary to preserve fidelity in low-noise data signals.

6.5 SWaP-C Analysis of GaN Converters

All of the components used on these PoL drop-on modules are COTs components. The total board utilized 14 capacitors, 11 resistors, 2 thermal straps, and 1 inductor which equates to a total of 28 passive components. The boards also had a total of 5 diodes and two GaN HEMTs and a single COTs controller. These package sizes ranged from 0201 to 0805 packages for passive components and 0201 to DO-214AC. Utilizing small common package sizes allows the designer to swap parts for the particular application with ease while maintaining low-cost components, but also eliminating unnecessary size and weight. The current board design for part purchasing is approximately 50-75 USD for necessary parts and part overages while board manufacturing is

about 500-1,000 USD depending on vendor qualifications. Time and materials have been eliminated from these estimations.

In summary, the TPS50601A-SP costs about $2,400 per chip which is about two to four times more expensive than the GaN converter. The TPS50601A-SP also has limited inventory due to its niche application area whereas the GaN converters utilize radiation tested controller and HEMTs that can be supplied by multiple vendors. Lastly, the power density of the GaN converters is almost double that of the TPS50601A-SP with better transient performance, and substantial improvements to the overall system efficiency.

7.0 Conclusions

This paper presented the shortcomings of radiation-hardened converters in current small space mission applications. Next, the benefits of GaN HEMTs and the importance of power density in future space missions were discussed. Then, the selection of GaN HEMTs, controller characteristics, the circuit topology was discussed. Following the part selection, layout and converter design optimizations were elaborated on to increase efficiency, reduce parasitics and enhance thermal performance associated with the three switching converters. Subsequently, the converter simulation results were presented for various scenarios. These simulation results were then compared with experimental results where the experimental tests matched similar trends to the simulation. Additionally, the power dense GaN Converters were compared directly to a popular radiation-hardened converter known as the TPS50601A-SP.

The benefits of the proposed radiation-tolerant high-power density drop-on PoL converters are evident when compared to radiation-hardened modules like the TPS50601A-SP. These radiation-tolerant converters offer a reduced mechanical footprint, higher switching frequency, improved output power capabilities, while a reduction in total converter cost.

Bibliography

[1]   Adriano Camps, "Nanosatellites and Applications to Commercial and Scientific Missions," 2019.

[2]   C. W. Stephanie DelPozzo, Lorena Carapacica, and Davin Gerber, "Nano/Microsatellite Market Forecast, 10th Edition," 2020.

[3]   Bhavya Lal *et al.*, *Global Trends in Small Satellites*. 2017.

[4]   C. M. Wilson *et al.*, "uCSP: A Diminutive, Hybrid, Space Processor for Smart Modules and CubeSats," 2016.

[5]   VPT Inc. "Space DC/DC Converters." https://www.vptpower.com/vpt-products/space-grade-dc-dc-converters/ (accessed.

[6]   Renasas. "Rad Hard Switching Regulators." https://www.renesas.com/us/en/products/space-harsh-environment/rad-hard-hermetic/rad-hard-power/rad-hard-switching-regulators (accessed.

[7]   Texas Instruments. "TI Space Products." https://www.ti.com/lit/sg/slyt532h/slyt532h.pdf?ts=1631426312631 (accessed.

[8]   J. Y. Tsao *et al.*, "Ultrawide-Bandgap Semiconductors: Research Opportunities and Challenges," *Advanced Electronic Materials,* vol. 4, no. 1, p. 1600501, 2018, doi: https://doi.org/10.1002/aelm.201600501.

[9]   Efficient Power Conversion, "EPC2030," *Datasheet,* pp. 1-6, 2020.

[10]   Efficient Power Conversion, "EPC2218," *Datasheet,* pp. 1-6, 2020.

[11]   GaN Systems, "GS61008T," *Datasheet,* pp. 1-17, 2020.

[12]   Thomas Cook, Aidan Phillips, Christopher Siak, Brandon M. Grainger, and Alan D. George, "Evaluation of Point of Load Converters for Space Computational Loads," in *2020 IEEE Aerospace Conference*, 7-14 March 2020 2020, pp. 1-12, doi: 10.1109/AERO47225.2020.9172360.

[13]   Thomas Cook, Nicholas Franconi, Bradley Shea, Christopher Wilson, Brandon M. Grainger, and Alan D. George, "Radiation-Tolerant, GaN-based Point of Load Converters for Small Spacecraft Missions," presented at the 32nd Annual AiAA/USU Conference on Small Satellites, 2018. [Online]. Available: https://digitalcommons.usu.edu/cgi/viewcontent.cgi?article=4138&context=smallsat.

[14]   A. Syed Khaja, "Diffusion Soldering for High-temperature Packaging of Power Electronics," 2018.

[15]   A. C. V. Bôas *et al.*, "Assessment of Ionizing Radiation Hardness of a GaN Field-Effect Transistor," in *2019 34th Symposium on Microelectronics Technology and Devices (SBMicro)*, 26-30 Aug. 2019 2019, pp. 1-4, doi: 10.1109/SBMicro.2019.8919340.

[16]   C. Nieto and R. Emami, "CubeSat Mission: From Design to Operation," *Applied Sciences,* vol. 9, p. 3110, 08/01 2019, doi: 10.3390/app9153110.

[17]   Texas Instruments, "TPS50601A-SP," pp. 1-36, 2019.

[18]   D. Reusch, "High Frequency, High Power Density Integrated Point of Load and Bus Converters," PhD, Electrical Engineering, Virginia Tech, 04/16/2012, 2012.

[19]   Linear Technologies, "LTC7800," *Datasheet,* pp. 1-32, 2020.

[20]   GaN Systems, "Design with GaN Enhancement mode HEMT," pp. 1-46, 2016.

[21]   Ansel Barchowsky *et al.*, "Analytical and experimental optimization of external gate resistance for safe rapid turn on of normally off GaN HFETs," in *2017 IEEE Applied Power Electronics Conference and Exposition (APEC)*, 26-30 March 2017 2017, pp. 1958-1963, doi: 10.1109/APEC.2017.7930966.

[22]   Nicholas Franconi, Alan D. George, Alessandro D. Geist, and Dennis Albaijes, "Signal and Power Integrity Design Methodology for High-Performance Flight Computing Systems," presented at the 2021 IEEE Space Computing Conference (SCC), 2021. [Online]. Available: http://doi.ieeecomputersociety.org/10.1109/SCC49971.2021.00011.